Hydrographic responses to regional covariates across the Kara Sea

Jussi Mäkinen [1], Jarno Vanhatalo [2,3]

[1] Department of Environmental Sciences, University of Helsinki, Finland
[2] Department of Mathematics and Statistics, University of Helsinki, Finland
[3] Department of Biosciences, University of Helsinki, Finland

Corresponding author: Jussi Mäkinen (jussi.makinen@helsinki.fi)

Key Points:

- We study the spatiotemporally varying surface hydrography and its relation to bathymetry, sea ice concentration, Arctic oscillation index and river Yenisei discharge with a spatiotemporally explicit hierarchical statistical model

- We show that the response of surface hydrography to environmental covariates in the Kara Sea varies spatially

- Our results show a positive trend of sea surface temperature and a negative trend of sea surface salinity between years 1980 and 2000 in the Kara Sea

Abstract

The Kara Sea is a shelf sea in the Arctic Ocean which has a strong spatiotemporal hydrographic variation driven by river discharge, air pressure and sea ice. There is a lack of information about the effects of environmental variables on surface hydrography in different regions of the Kara Sea. We use a hierarchical spatially varying coefficient model to study the variation of sea surface temperature (SST) and salinity (SSS) in the Kara Sea between years 1980 and 2000. The model allows us to study the effects of climatic (Arctic oscillation index, AO) and seasonal (river discharge and ice concentration) environmental covariates on hydrography. The hydrographic responses to covariates vary considerably between different regions of the Kara Sea. River discharge decreases SSS in the shallow shelf area and has a neutral effect in the northern Kara Sea. The responses of SST and SSS to AO show the effects of different wind and air pressure conditions on water circulation and hence on hydrography. Ice concentration has a constant effect across the Kara Sea. We estimated the average SST and SSS in the Kara Sea in 1980-2000. The average August SST over the Kara Sea in 1995-2000 was higher than the respective average in 1980-1984 with 99.9 % probability and August SSS decreased with 77 % probability between these time periods. We found a support that the winter season AO has an impact on the summer season hydrography, and temporal trends may be related to the varying level of winter season AO index.

Index terms

4207 Arctic and Antarctic oceanography

4271 Physical and chemical properties of seawater

1635 Oceans

1986 Statistical methods: Inferential

1990 Uncertainty

Keywords

Sea surface hydrography, Bayesian hierarchical model, Gaussian processes, oceanography, spatiotemporal, Arctic shelf sea

1 Introduction

The Arctic Ocean is subject to decreasing cover and volume of sea ice, increasing sea surface temperature (SST) and changes in sea surface salinity (SSS) [McPhee et al., 2009; Steele et al., 2008; Stroeve et al., 2007]. We need more accurate predictions of surface hydrography as it acts in an interplay with Arctic ice cover and affects the climate and weather conditions in the Arctic and in the mid-latitudes [Bingyi and Jia, 2002; Petoukhov and Semenov, 2010]. In addition to climatology also biological production and marine species distributions are affected by surface hydrography [Fetzer, Hirche and Kolosova, 2002; Moore and Huntington 2008]. Here we study the spatiotemporal variation of SST and SSS in the Kara Sea from 1980 until 2000. We use *in situ* observations and hierarchical statistical models to study the impact of climatic (Arctic oscillation index) and seasonal (river discharge and ice concentration) environmental covariates on the surface hydrography of the Kara Sea.

The Kara Sea is one of the shelf seas surrounding the Arctic Basin (Fig. 1). Its hydrography is characterized by fresh water inflow from the continental rivers and saline water inflow from the Barents Sea [Pavlov and Pfirman 1995], which together with seasonal ice conditions cause strong spatiotemporal hydrographic variation [Janout et al., 2015]. During the past few decades in the Kara Sea, ice concentration has declined and SST increased, which have resulted from strengthened heat flux through Atlantic currents and enhanced warm air flow from the mid-latitudes [Gerdes 2003; Polyakov et al., 2007]. Furthermore, increased river discharge has enhanced heat flux especially in the shallow shelf areas [Steele et al., 2008], but has also reduced the general level of SSS [Peterson et al., 2002; Steele and Ermold 2004]. All these changes affect the biota in a manner that is difficult to predict [Doney et al., 2012]. There is also an increasing interest on the Kara Sea as a shipping route and oil and gas reservoir, which create an environmental threat on the local biota [Ho 2010, Nevalainen et al., 2016]. Hence, there is a growing interest in the current and past environmental conditions of the Kara Sea and of the Arctic shelf seas in general.

Despite earlier efforts, we lack spatially and temporally accurate information about surface hydrography in the Kara Sea. The circulation studies of Harms and Karcher [1999; 2005] explained seasonal circulation patterns, and Panteleev et al. [2007] explained inter annual variation of the circulation patterns in relation to the Arctic oscillation (AO). Steele and Ermold [2004] and Steele et al. [2008] studied broader scale trends of SSS and SST, respectively, and investigated temporal trends from the last 100 years in the Pan-Arctic region. However, the studies were carried out in a low spatial resolution and temporal trends were left without an assessment of the total uncertainty.

In this study we use hierarchical statistical models to study the spatiotemporal patterns of the surface hydrography. The novelty of the study is in the spatially varying responses of surface hydrography to environmental covariates. We also estimate the SST and SSS patterns from 1980 to 2000 and quantify the uncertainty related to these estimates.

2 Study area

The Kara Sea (Fig. 1) is a shallow shelf sea (the mean depth is 111 meters and 40% of the sea area is shallower than 50 meters), where warm Atlantic, cold Arctic and fresh river inflow mix [Pavlov and Pfirman 1995]. Sea currents transport relatively warm and salty Atlantic water to the western part of the Kara Sea through the Kara Strait and around the northern tip of Novaya Zemlya (NZ). The northern Kara Sea receives salty Atlantic water from a current heading north along the St. Anna Trough [McClimans et al., 2000; Schauer et al., 2002]. Fresh water is transported to the Kara Sea in larger extent through the rivers Ob and Yenisei, which make 40 % of the total river run-off to the Arctic Ocean, and to a lesser extent through the rivers Nizhnanyaya and Pyasina, which are located eastward from the river Yenisei [Ruediger 2003]. River discharge peaks in May and June and stays low outside of the summer season.

The Kara Sea is annually covered by sea ice. Ice formation starts in September and complete ice cover lasts from November to June. Ice formation creates brines and especially polynyas are prone to continuing ice formation and are a source of saline water [Martin and Cavalieri 1989; Pavlov and Pfirman 1995]. Wind and ice motion create horizontal stress on sea surface, which controls fresh water distribution and export from the Kara Sea [Panteleev et al., 2007].

Sea surface temperature stays below 4 °C throughout the year, except in estuaries where it may peak at 9 °C. Summer temperatures decrease in the northeast direction but in winter surface water is constantly at the freezing point as the whole sea is covered by ice [Pavlov and Pfirman 1995]. Salinity increases from east to west with the strengthening impact of the Atlantic water. Ice formation, ice export and river discharge control local scale variation of salinity [Harms and Karcher 1999]. The location of fresh water dominance is controlled by wind conditions [Johnson et al., 1997].

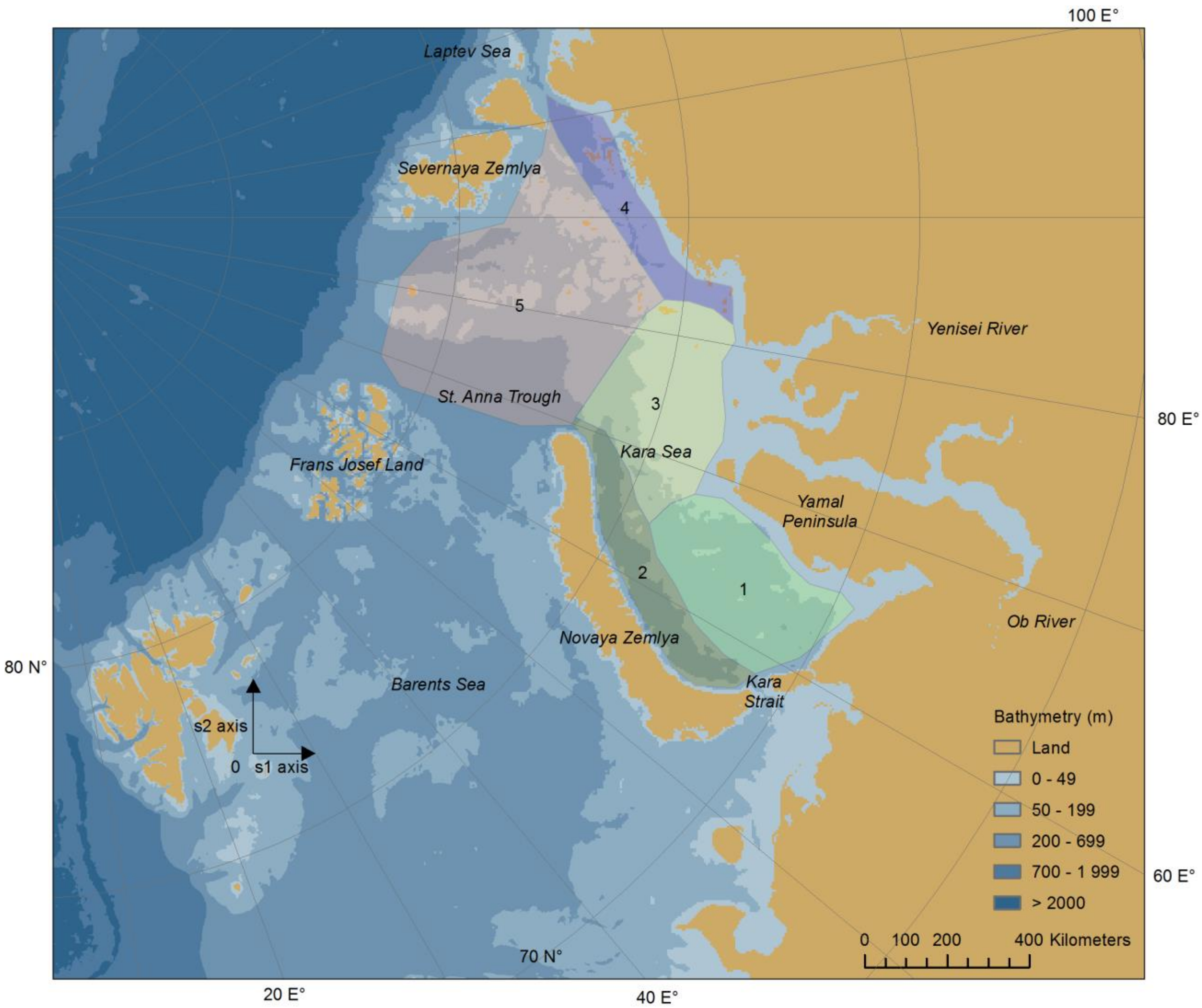

Figure 1. The Kara Sea and its division into five sub regions in relation to its physical characteristics. The s_1- and s_2-axis denote the axes of the coordinate system used in the analysis and in Fig. 2 and 3. The intersection of these axes denotes the origo for the distances in Fig. 2 and 3.

The Kara Sea is divided into five regions with different physical characteristics (Fig. 1).The southwestern corner (Region 1) has the highest annual temperature and is affected by Atlantic current through the Kara Strait [Pavlov and Pfirman 1995]. Eastern coast of NZ (Region 2) is affected by strong ice formation and oceanic current flowing to southwest [Pfirman 1995]. The region in front of the river estuaries (Region 3) is affected by annual pulses of fresh water [Harms and Karcher 2005]. The northeastern coast (Region 4) is an outflow path for fresh water export to the Laptev Sea [Janout et al., 2015]. The northern Kara Sea (Region 5) is influenced by Atlantic currents and flow from the southern Kara Sea [Pavlov and Pfirman 1995].

3 Materials and methods

3.1. Data

The data comprises SST and SSS measurements, bathymetry, AO, discharge of the river Yenisei and sea ice concentration from 1980 to 2000; the time period spanned by all the data sources. Bathymetry varies in space, AO and discharge in time, and ice concentration in space and time. The results are presented and the hydrographic estimates generated in a lattice grid with 5 km cell size. This resolution was chosen as a compromise between computational effort and good visual mapping.

Hydrographic measurements of SST and SSS were compiled from World Ocean Data Base (WOD) 2013, which integrates quality controlled oceanographic data sets from several sources ([Boyer et al., 2013; NOAA, OCL], see also Fig. 1 in supplementary material). We did not include remote sensed satellite data into the analysis. Most of the available high resolution satellite data start from the 2000s' [Stroh et al., 2015]. The high resolution OISST data set is available from 1981 but the data set is an interpolation derived by analyzing satellite images and point observations from ships and buoys [Reynolds et al., 2007]. Hence, we would have data point duplicates between OISST data set and the point observations from the WOD. Moreover, satellite images do not detect SST through ice and hence would not have improved the input data in the season of sea ice cover when there is a shortage of point observations.

The environmental variables were selected based on their assumed impact on hydrography and their accessibility. Bathymetric data was derived from the International Bathymetric Chart of the Arctic Oceans (IBCAO v. 3.0) [NOAA, NGDC], which is generated from ship track data, contour maps, gridded sources, topography and coastline information [Jakobsson et al., 2012]. The bathymetry data was transformed from the original 500 meters to 5 km resolution. Bathymetry is used to describe the effect of shallow shelf area on the hydrography. In general, the shallower the water column, the faster it heats up in the summer and affects SST. Furthermore, river discharge has the strongest impact in the shelf area and hence, bathymetry is an index for the effect of the fresh water.

AO describes the 1000mb height anomaly north from 20° N latitude. AO indicates the polar vortex modulation and contributes to the Arctic climate and oceanic sea level pressure. AO is a surrogate for the differences in air pressure systems on the northern hemisphere. It indicates the wind system, which regulates the sea currents in the Arctic [Thompson and Wallace 1998; Rogers and McHugh 2002]. The AO data set is archived by and accessible through Climate Prediction Center of NOAA [NOAA, CPC]. We utilized the monthly mean values of AO. Water circulation patterns change in the Kara Sea according to the prevailing AO regime [Panteleev et al., 2007]. The AO regime used in the literature describes air pressure conditions which last from a couple of months to decades. We included the monthly mean AO and the mean AO over the previous winter (from December to March) into the analyses. The former explains the monthly scale water circulation patterns and its effects on the hydrography and the latter describes the mean air pressure conditions of the past winter, which affect the hydrographic conditions of the following spring, summer and autumn through ice transport and formation. Especially in the Kara Sea, AO is an important factor affecting the summer season sea ice conditions [Rigor et al., 2002; Rigor and Wallace 2004].

Discharge values were measured from the river Yenisei in a gauge situated 697 kilometers inland from the river pour point. Of the two major rivers, Yenisei and Ob, we selected Yenisei to represent the continental fresh water inflow for its higher discharge and relatively short estuary zone. The rivers Ob and Yenisei vary seasonally in a similar manner. Since our model is correlative and does not describe causal effects of different discharge pathways from Yenisei or Ob, having two covariates with similar variation would not improve the model performance. The river discharge data has been utilized by earlier studies [Shiklomanov and Lammers 2009] and is accessible through R-ArcticNet [R-ArcticNet]. We counted a mean daily discharge for each month based on the daily discharges. We took the logarithm of the discharge in order to lower the discharge peak in May and June and to improve the fit of linear response compared to using discharge directly. We tested the effect of time lag on the impact of discharge on hydrography. Based on the model comparison (see Section 3.2 and Appendix B) we selected a two months lag to describe the time needed for discharge to affect hydrography.

The monthly mean sea ice concentration data was derived from the brightness temperature data from the National Snow & Ice Data Center [Cavalieri et al., 1996; NSIDC]. The ice concentration data were re-interpolated from 25 km cell size onto a 5 km cell size grid by using ordinary kriging interpolation. We used spherical semivariogram for modelling the distance decay and infer lag, nugget and sill with ArcMap software [ESRI 2015]. The re-interpolation smoothened rasters but did not incorporate new data to improve the accuracy.

3.2. Spatiotemporal modeling with spatially varying coefficient processes

We built a hierarchical Bayesian spatiotemporal regression model for both end variables (SSS or SST). The regression model was then used to examine the effects of environmental covariates (bathymetry, ice concentration, monthly mean AO, winter mean AO and log of the river Jenisei discharge) on SST and SSS and to estimate SST and SSS over the Kara Sea at the 5 km grid cells from 1980 to 2000.

Let $y(\boldsymbol{s},t)$ and $\boldsymbol{x}(\boldsymbol{s},t)$ denote respectively the end variable and the vector of 5 environmental covariates at location $\boldsymbol{s}$ (coordinates in km) and time t (in years). Notice that AO and log river discharge covariates vary in time but not in space, bathymetry is constant over time but varies in space, and ice concentration varies in time and space. We followed Gelfand et al. [2003] and used a spatially varying coefficient process independently for both end variables

$$y(\boldsymbol{s},t) = \alpha(\boldsymbol{s},t) + \boldsymbol{x}(\boldsymbol{s},t)^{\boldsymbol{T}}\boldsymbol{\beta}(\boldsymbol{s}) + \varepsilon(\boldsymbol{s},t), \quad (1)$$

where $\alpha(\boldsymbol{s},t)$ is a spatiotemporally varying intercept, $\boldsymbol{\beta}(\boldsymbol{s}) = [\beta_1, \beta_2(s) \dots, \beta_5(s)]^T$ is a 5×1 vector of one constant and four spatially varying coefficients and $\varepsilon(\boldsymbol{s},t)$ is the i.i.d. zero mean Gaussian observation error with variance parameter σ_ε^2. Different from the ordinary linear regression, where the linear coefficients are assumed constant in space ($\beta_d(s) = \beta_d$ for all s), the spatially varying coefficient process assumes that the coefficients are (latent) functions of the spatial coordinates. Hence, the model is an extension to the traditional linear regression so that we allow the response of SST and SSS along covariates to change in space. Moreover, the intercept is allowed to vary in space and time leading to spatiotemporally varying intercept which accounts for temporally and spatially correlated variation that is not explained by the covariates.

We assumed that the coefficients related to ice concentration, monthly mean AO, winter mean AO and river Yenisei discharge, respectively $\beta_2(s) \dots, \beta_5(s)$, vary in space and the coefficient related to bathymetry, β_1, is constant throughout the study region. We standardized all the covariates to have zero mean and standard deviation of one in order to help the assessment of their relative importance for explaining the data. We standardized also the end variables, y, to have zero mean and standard deviation of one for modeling and retransformed them to the original scale when presenting results.

We followed the Bayesian approach [Gelman et al., 2014] and gave a vague Gaussian prior for the constant coefficient related to the bathymetry, $\beta_1 \sim N(0,10)$, and independent Gaussian process (GP) priors [Gelfand et al., 2003] for the spatiotemporally varying intercept and spatially varying regression coefficients, $\beta_d(\boldsymbol{s})$, where $d \in \{2,3,4,5\}$. A GP is a stochastic process that can be used to define distributions over functions. It is defined by a mean and a covariance function so that, e.g., $\beta_2(\boldsymbol{s}) \sim GP(0, k(\boldsymbol{s}, \boldsymbol{s}'))$ denotes that the coefficients corresponding to the second covariate have a zero mean GP prior with a covariance function $k_2(\boldsymbol{s}, \boldsymbol{s}') = Cov[\beta_2(\boldsymbol{s}), \beta_2(\boldsymbol{s}')]$ that describes the correlation between coefficients at locations $\boldsymbol{s}$ and $\boldsymbol{s}'$. We assumed that the three coefficient processes are mutually independent and have zero mean GP priors with exponential covariance functions, so that the covariance function of the d^{th} coefficient process is $k_d(\boldsymbol{s}, \boldsymbol{s}') = \sigma_d^2 e^{-\sqrt{\sum_{i=1}^{2} (s_i - s_i')^2 / l_{d,i}^2}}$. The variance parameter, σ_d^2, governs the magnitude of the regression coefficients and the length-scale parameters, $l_{d,i}$, govern the autocorrelation length of the GP along the x- and y-coordinates (Fig. 1). The correlation between two locations drops below 5% of its maximum when these locations are approximately three times the length scale apart. Hence, the exponential covariance function implies continuous functions for the coefficients and that the coefficients at alternative locations are the more correlated the closer they are in space. The coordinate system for the spatial processes was chosen to reflect the main directions of the Kara Sea so that x axis corresponds roughly to the distance from the continent (see Fig. 1).

The spatiotemporally varying intercept is given a GP prior with mean $\alpha_0 \sim N(0,10)$ and an additive covariance function of three components. The first component is an exponential covariance function of spatial location $k_{\text{exp}}(\boldsymbol{s}, \boldsymbol{s}') = \sigma_{\text{exp}}^2 e^{-\sqrt{\sum_{i=1}^{2} (s_i - s_i')^2 / l_{\text{exp},i}^2}}$ (similar to the covariance functions of the regression coefficients) and it corresponds to a temporally constant process that describes spatially varying long term averages over the study period. The second component is a product of exponential covariance function in space and a periodic covariance function in time, $k_{\text{perST}}((\boldsymbol{s}, t), (\boldsymbol{s}', t')) = \sigma_{\text{perST}}^2 e^{-\sqrt{\sum_{i=1}^{2} (s_i - s_i')^2 / l_{\text{perST},i}^2}} e^{-\sqrt{2 sin^2(\pi |t - t'|) / l_{\text{perST},3}^2}}$. This component describes seasonally varying spatial patterns in the intercept that recur annually. The last component is a product of exponential covariance function in space and exponential covariance function in time, $k_{\text{expST}}((\boldsymbol{s}, t), (\boldsymbol{s}', t')) = \sigma_{\text{expST}}^2 e^{-\sqrt{|t - t'| / l_{\text{expST},3} + \sum_{i=1}^{2} (s_i - s_i')^2 / l_{\text{expST},i}^2}}$, which captures spatiotemporal variation that does not have seasonal pattern. This covariance structure leads to an additive model where each covariance function corresponds to one spatiotemporal process [Rasmussen and Williams, 2006].

After formulating the model we trained it with the data by applying the Bayes rule and calculating the posterior distribution over the model parameters (e.g., parameters of the covariance functions) and the latent coefficient functions. The trained model was then used to calculate the posterior probability distribution for SSS and SST at all grid cells for each month from 1980 to 2000 (see Supplementary material for maps summarizing these). These posterior distributions were used to calculate areal and temporal averages. All the calculations were conducted with GPstuff toolbox [Vanhatalo et al., 2013]. See Appendix A for more details on the model and its training as well as the posterior results for the hyperparameters. The models were validated with the posterior predictive checks [Gelman et al., 2014] and leave-one-out cross validation (LOO-CV, Vehtari and Ojanen, 2012). See Appendix B for details.

4 Results and discussion

4.1. The effects of covariates on SSS

Both AO indices, discharge of Yenisei and ice concentration have a significant and spatially varying effect on SSS (Fig. 2, 3) whereas bathymetry does not have any effect (its posterior mean was -0.01 and its 95 % credible interval is between -0.06 and 0.03). River discharge has a negative impact on SSS over most of the study area so that the magnitude of the response decreases to west and north. This is reasonable since river discharge increases the fresh water content in the central Kara Sea. Only the southwestern corner has a positive response to river discharge which may be due to an increased transport of saline water from the Barents Sea to the Kara Sea during the positive monthly AO, which is coupled with high river discharge [Panteleev et al., 2007]. The effect of ice concentration on SSS is mostly positive in the Kara Sea and strongest in the central part. Ice formation increases SSS and correlates negatively with discharge of fresh water. During winter the discharge of fresh water does not compensate the year round operating saline Atlantic water inflow which leads to an increase of SSS [Harms and Karcher 1999]. Ice concentration has a negative effect on SSS only in the southwestern corner, which may be related to some local hydrographic process that we could not take into account with the model parameters.

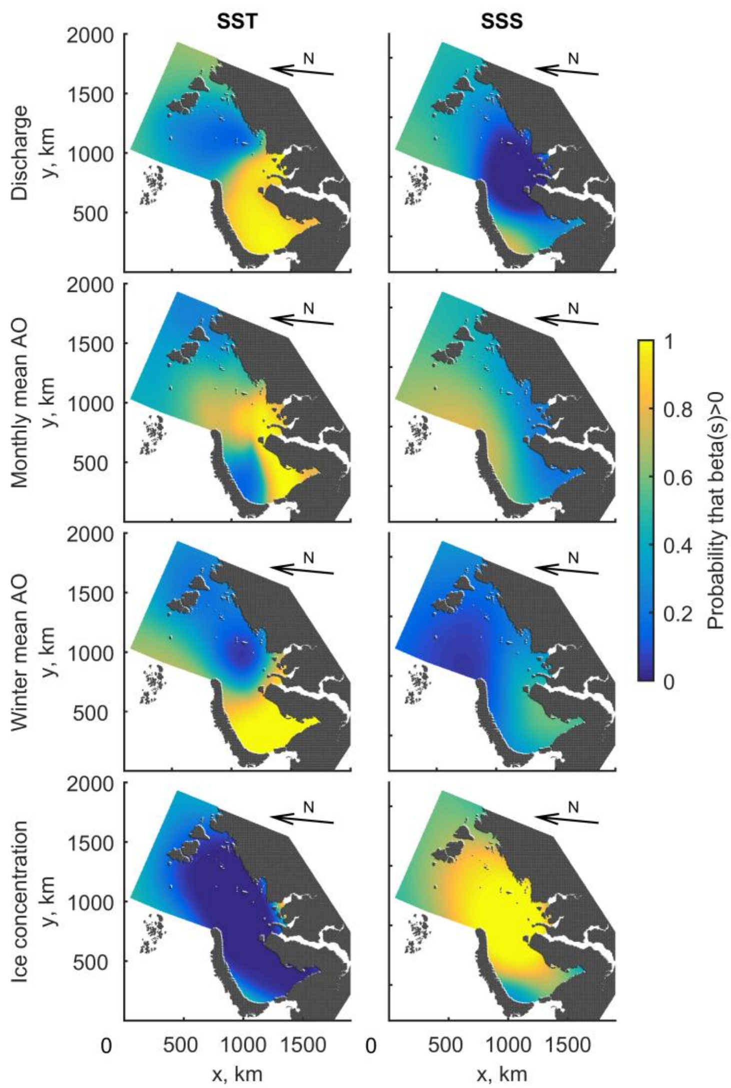

Figure 2. The spatially varying coefficients of SSS and SST. The maps show the probability that the spatially varying coefficient is positive.

The coefficients of both AO indices vary spatially (Fig. 2, 3). Monthly mean AO has negative coefficients on the shelf area and positive coefficients in the northwestern Kara Sea. During negative phase of monthly mean AO the easterly winds prevail, which creates a weaker circulation pattern: saline currents from the Barents Sea and from the Arctic Ocean entering the northern Kara Sea are depressed and the saline current along the eastern coast of NZ is reduced. Also the fresh water current out from the Kara Sea along the northeastern coast declines [Janout et al., 2015; Panteleev et al., 2007]. These are called blocking conditions because of the reduced levels of saline water inflow and fresh water export. The positive coefficients of monthly mean AO in the northwestern Kara Sea indicate an intensified inflow of saline Atlantic water during positive monthly mean AO [Panteleev et al., 2007]. In the northeastern coast negative coefficients in turn reflect the strengthened fresh water export to the Laptev Sea [Harms and Karcher 2005]. The southeastern Kara Sea has a negative response to monthly mean AO. During negative monthly mean AO northeasterly wind pattern pushes water from the southcentral Kara Sea to the southern corner. According to the circulation study of Panteleev et al. [2007], such a mechanism would cause relatively saline water to accumulate there.

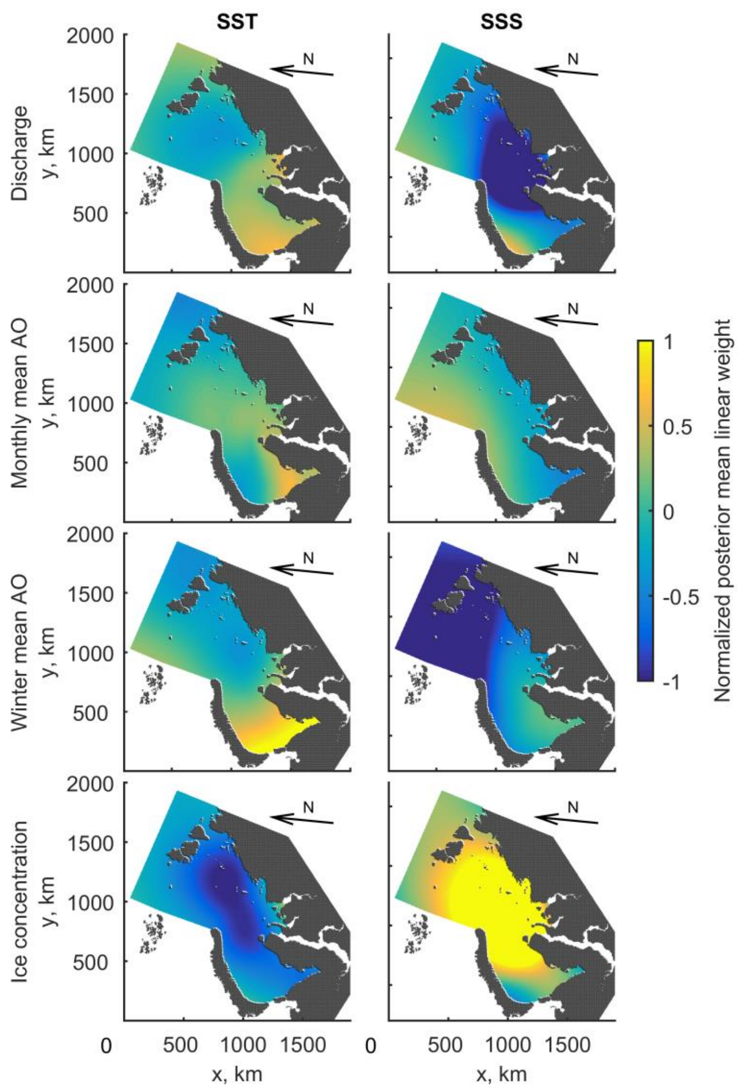

Figure 3. The spatially varying coefficients of SSS and SST. The maps show the normalized posterior mean of linear weight.

As the monthly mean AO index is a surrogate for wind pattern, the mean winter AO indicates the impact of the past winter meteorological conditions on the hydrography of the following spring, summer and autumn. AO index varies more strongly in winter than in summer and affects the ice transport and the hydrography of the following year [Rigor et al., 2002]. The two AO indices impact in different temporal scales. SSS has a negative response to winter mean AO in most parts of the Kara Sea, as only the southern part has a neutral response. During a negative winter AO the ice export decreases and the following spring and summer are characterized by higher sea ice concentration and volume, and lower SST and air surface temperatures. Furthermore there is an intensified sea ice formation in the following autumn leading to higher ice volume [Rigor et al., 2002]. Stronger ice formation would increase SSS and negative winter mean AO would affect positively SSS. In the southern Kara Sea ice conditions may be less affected by ice transport to the Arctic Ocean and the response to the winter mean AO is neutral. The winter mean AO describes, thus, the severity of ice conditions in the Kara Sea which cannot be fully captured by the ice concentration that does not directly account for ice volume. In addition to ice conditions the winter mean AO indicates also the water circulation patterns in the Arctic Ocean, which affects also the northern Kara Sea [Morison et al., 2000; Morison et al., 2006]. The negative response of SSS in the northern Kara Sea results from a decreased freshwater content in the Eurasian basin under an anticyclonic circulation pattern (negative AO) [Morison et al., 2012]. The change in the response from neutral to strongly negative is along the shelf break where the Arctic circulation pattern starts to affect hydrography [Morison et al., 2012].

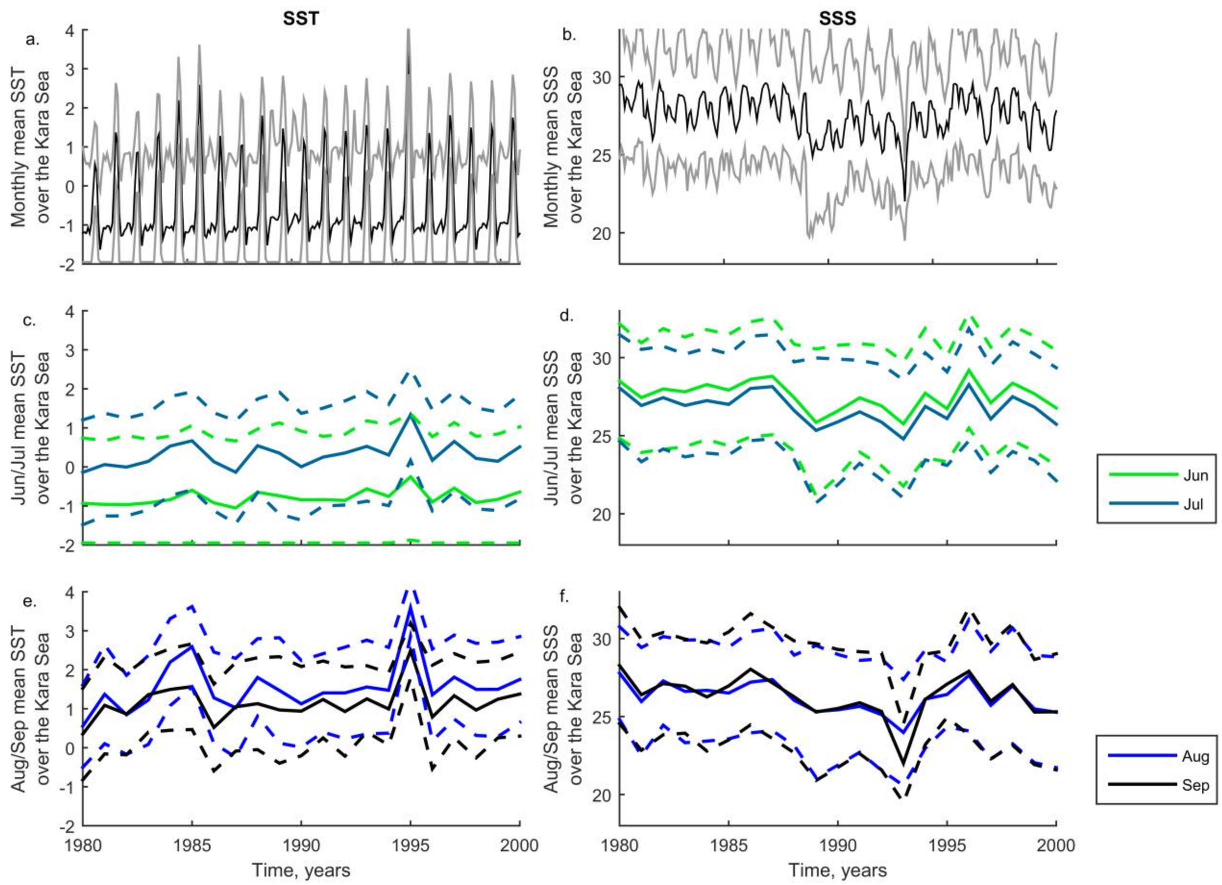

Figure 4. The annual variation of SST and SSS over the whole Kara Sea. Plots a-b) show the posterior mean (black line) and 95% credible interval (light grey line) of each study month. Plots c-d) and e-f) show the posterior mean and 95% credible interval of early (June and July) and late summer months (August and September), respectively.

It should be noted that the model does not uniquely indicate causality and hence the coefficients may represent mere correlation with causal drivers. An assumption of causality between river discharge and SSS in the central Kara Sea seems justified. The coefficients are weaker further away from the estuaries and outside of the shelf region. The negative responses continue along the northeastern coast, which is a pathway of fresh water export from the Kara Sea [Harms et al., 2005;

Janout et al., 2015]. River discharge is a seasonal process which follows an annual pattern peaking in May and June (Fig. 4 in supplementary material). Still, some part of the negative response may be related to ice melt driven decrease of SSS in summer after the discharge peak. The southern corner of NZ has a controversial response to discharge and sea ice which may be caused by a local factor not included in the model. This could be, for example, a local scale saline current from south which is intensified during the years of positive AO regime [Panteleev et al., 2007].

The spatiotemporal variation of SSS is explained by variables operating in different spatial scales and having causal and correlative effects. As river discharge and ice concentration can be interpreted to have a causal relationship on the hydrography, both AO indices correlate with climatological variation and control circulation patterns which have a causal relationship with the hydrography [Panteleev et al., 2007; Rigor et al., 2002]. The impact of discharge and ice concentration is mostly unidirectional and only the magnitude of the impact varies in the Kara Sea. AO indices on the contrary correlate with climatic factors that drive circulation patterns in multiple scales. These circulation patterns may have different effects on the surface hydrography in different regions in the Kara Sea. Positive AO regime drives an eastward wind pattern and saline water penetration from the Atlantic, which increases the average SSS in the Kara Sea [Harms and Karcher 1999; Panteleev et al., 2007]. On the other hand the positive AO regime is characterized by higher precipitation on the continent and higher discharge in continental rivers [Peterson et al., 2002]. Hence, positive mean monthly AO correlates with lower SSS and higher fresh water export along the northeastern coast. The responses of SST and SSS are linked to the effects of AO on the water circulation, which is highlighted with the strongly negative responses of SSS to mean winter AO in the northern Kara Sea [Morison et al., 2000; Morison et al., 2012].

The mean winter AO correlates with the summer ice concentration [Rigor et al., 2002]. As it indicates the mean conditions of the winter, it sums up a larger scale atmospheric pressure conditions than the monthly mean AO. The different coefficients in the northern and southern Kara Sea indicate regionally different effects on SSS. Accordingly winter mean AO explains a part of variation of SSS which is not explained by ice concentration only but is also related to ice volume. The high volume of sea ice transport from the northern Kara Sea, higher surface air temperature and less intensive ice formation decrease SSS. As the coefficients of monthly mean AO varied in a west-east direction, the coefficients of winter mean AO varied in a north-south direction. There are different drivers of SSS correlating with different AO indices.

The monthly average ice concentration of the Kara Sea is significantly correlated with mean monthly AO (corr. -0.5301). There was not significant correlation between monthly mean AO and monthly mean daily river discharge (corr. = 0.0303). We found a stronger correlation between the annual median AO and the annual sum of river discharge (corr. = 0.3506). This was expected as the multiannual variation of AO affects the precipitation and river discharge in high latitudes [Peterson et al., 2002]. The mean winter AO and annual sum of discharge were even more strongly correlated (corr. = 0.3961). The winter mean AO catches more of the long term variation of AO than the monthly mean index. There was also a correlation between annual mean ice concentration and winter mean AO (corr. -0.4169).

4.2. The effects of covariates on SST

The 95 % posterior credible interval of the coefficient of bathymetry is between 0.07 and -0.01 and its posterior mean was 0.03. Hence, bathymetry has a positive effect on SST as assumed. SST increases in the shelf area compared to the deep sea. The response of SST to ice concentration is constantly negative, since ice concentration is highly correlated with winter season and cold surface air temperatures (Fig. 2, 3). The most negative coefficients are concentrated in the central Kara Sea, where the uprising of warm Atlantic water prevents the formation of constant ice cover and creates polynyas [Anselme 1988]. Under these conditions low ice cover is an index for warm water uprising and an increase of SST.

The response of SST to river discharge varies spatially. Discharge has a positive effect on SST in the southern Kara Sea and a negative effect in the northern Kara Sea and along the northeastern coast line. Discharged water induces water column stratification which accelerates surface cooling and ice formation in autumn. The northeastern coast is affected by fresh water more than the southern Kara Sea, where stratification is weaker [Harms and Karcher 1999]. The positive responses in the southern Kara Sea may be related to seasonality.

In general the effects of wind patterns and water circulation on SST are less studied than on SSS. SST in the south corner of the Kara Sea has a positive response to monthly mean AO. Positive monthly mean AO is characterized by inflow of relatively warm Atlantic water through the Kara Strait, which increases SST in the southern Kara Sea [Zhang, Rothrock, and Steele 1998]. The cyclonic circulation pattern of the Kara Sea during positive monthly mean AO may enhance SST in the estuary region. The negative responses to the monthly mean AO in the northern parts and close to the NZ in the south Kara Sea are related to warm water accumulation due to blocking conditions during negative AO, which increases SST [Panteleev et al., 2007].

The spatial pattern of the coefficients of the winter mean AO differs from that of the monthly mean AO. They are distributed in a decreasing pattern from south to north. The southern Kara Sea has a positive response to winter mean AO, which is due to the lower ice concentration, increased surface air temperature and increased Atlantic water inflow from the Barents Sea [Rigor et al., 2002; Morison et al., 2012]. As discussed earlier, the positive winter mean AO has an effect on the cyclonic water circulation pattern, which increases warm water inflow from the Barents Sea to the Kara Sea [Morison et al., 2012]. The northern Kara Sea on the other hand is dominated by negative response which is in conflict with the study of Rigor et al. [2002]. The higher ice transport and lower ice concentration should be coupled with increased SST throughout the Kara Sea. The negative responses may be related to Ekman pumping, which forces the warm surface water to diverge from the central and northern Kara Sea [Janout et al., 2015].

4.3. Temporal changes in SSS and SST

The Kara Sea consists of hydrographically different regions. There is more inter annual hydrographic variability in the regions 1-3 located on the shelf area than in the regions 3 and 5 in the deep sea area, which agrees with the finding of Simstich et al. [2005] (Fig. 5). The shelf area and the western Kara Sea are affected by inflows of fresh and saline water, respectively, as the northern part has more stable hydrographic conditions.

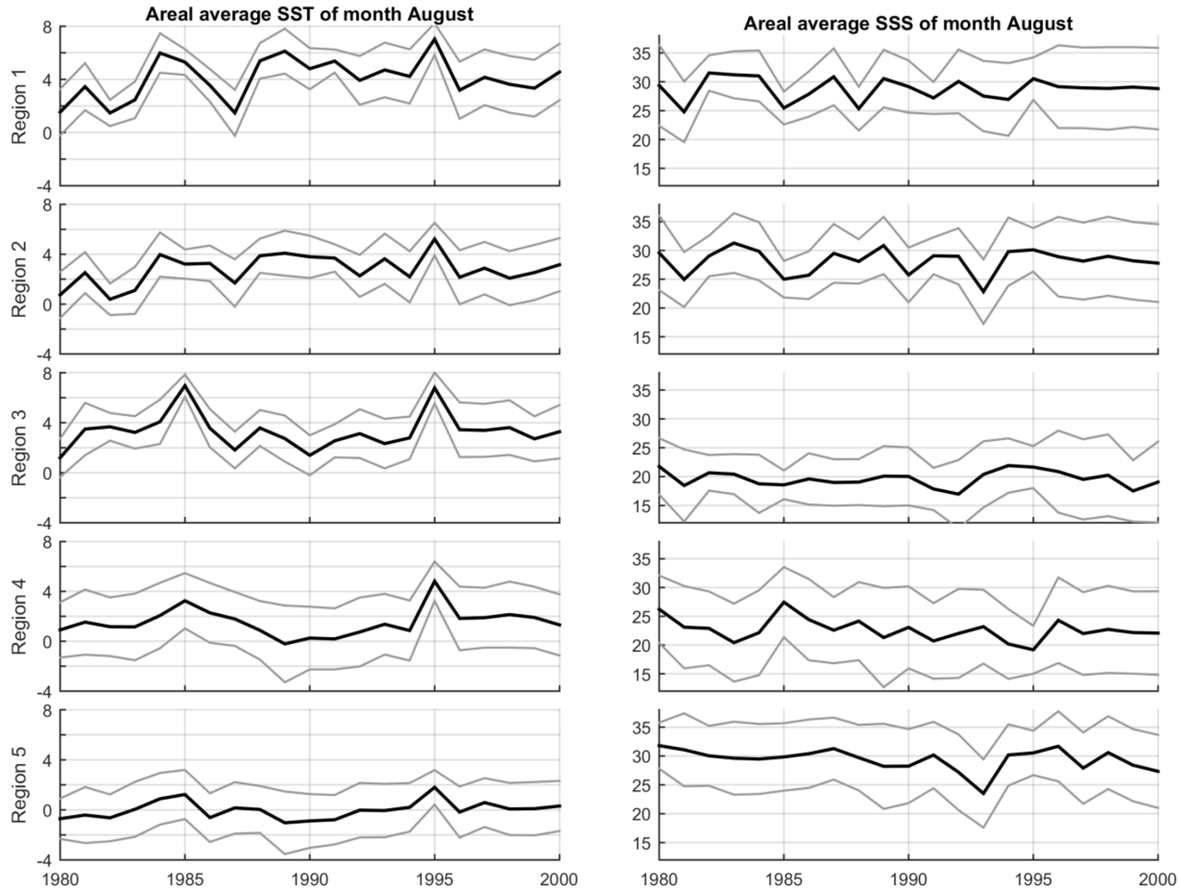

Figure 5. Areal mean SST and SSS of the month August of the Kara Sea sub regions. Black line shows the posterior mean and grey lines the central 95% credible interval.

The uncertainties related to hydrographic estimates make it difficult to assess temporal trends with high certainty (Fig 4, 5). This has been acknowledged in earlier studies, which have struggled with sparse data sets [Harms and Karcher 1999; Panteleev et al., 2007; Simstich et al., 2005]. The uncertainty in our model estimates depends on the spatial and temporal availability of observations so that uncertainty is the lowest at locations and times that are near the observation points and hence, summer seasons have lower uncertainties than winter seasons (Fig. 4). During winter and early summer the uncertainty is the highest and during this period of time the Gaussian distribution for the SST is slightly suboptimal since the posterior distribution gives non negligible probability mass to temperatures below the physical limit of approximately -1.85 °C (seen as 95% interval dropping below this limit in Figure 4).

We divided the study period into sub periods of five to six years and compared them pairwise. There is a probable increase of SST from the first study period (1980-1984) to the last one (1995-2000) in the month of August. The expected increase in August is 0.7 °C with 95% probability interval between 0.2 and 1.2 °C. This supports the results of Steele et al. [2008], who showed a significant increase of SST in the whole Arctic and in the Kara Sea in summer (July – September) in years 1965-1995. The year 1995 stands out with a summer season SST that was almost 2°C higher than the study period average in many sub regions (Fig. 5). The anomaly of the whole Kara

Sea is over 1.5 °C with a probability of 0.95. This extreme SST may result from high air surface temperatures in the Kara Sea region in and around the year 1995 [Lawrimore et al., 2011].

The probability that salinity has decreased between the first and the last sub period in August is 0.76. Large scale study of Steele and Ermold [2004] has shown a statistically significant freshening of the Kara Sea in the 30 years period between 1965 and 1995. Our study supports the results of Simstich et al. [2005] that suggested a gradual freshening of the whole water column between years 1996 and 2002 in the central Kara Sea. Our results show a decreasing trend of SSS after year 1995, which assumingly correlates with the freshening of the whole water column (Fig. 4).

The temporal changes of the average hydrographic conditions of the Kara Sea are probably related to climatic conditions. Both AO variables are straight indices of the climatic variation as ice concentration and discharge are affected by the climate. The changes of AO explain the variation of SSS and SST in multi decadal scales [Steele et al., 2004; 2008] and in shorter study periods [Panteleev et al., 2007; Rigor et al., 2002; Simstich et al., 2005]. Our study period consists of negative (1980-1988) and positive (1989-1995) AO regimes, when we compared the annual mean winter AO. The last period 1996-2000 shows strong annual fluctuations. With a probability of 0.8 there is an increase of the mean SST in month August between negative and positive AO regimes. During the same time SSS has decreased with a probability of 0.9. These results support the study of Rigor et al. [2002] about the effects of winter season AO on hydrography. In a multiyear scale the hydrographic variation follows the changes of AO with a time lag of a few years [Morison et al., 2006]. The high air surface temperatures and peaks of SST and SSS in 1995 are possibly caused by extremely high AO around 1989 and 1990, which increased the warm and saline water content in the Arctic Basin four to five years later [Morison et al., 2006; Steele and Boyd 1998].

Our results agree with previous studies about the importance of AO on SST and SSS, but we want to highlight the spatially varying impact of AO on the hydrography. The different regions of the Kara Sea respond in different ways to changes in winter mean AO and in monthly mean AO. Moreover, the effects come through changes in ice concentration and movements, water circulation patterns and continental river discharge [Pavlov and Pfirman 1995].

5 Conclusions

On the level of the whole Arctic there have been major changes in environmental conditions during the past decades. These affect also SST and SSS which are important factors for species communities and biological production. Hence, more detailed information on SST and SSS from the Arctic shelf sea is of practical information when, for example, predicting effects of climate change on marine biota. Our study concentrated on the Kara Sea. We analyzed the effect of key environmental variables on SST and SSS with hydrographic *in situ* measurements and model based statistical inference. Our spatially varying regression model allows the regression coefficients related to environmental covariates to vary spatially, which created an analytic way to study areal responses to environmental variables. However, the modelling approach used here is based on correlative relationships between hydrographic observations and spatially or spatiotemporally varying covariates but does not describe physical dynamics. This data driven methodology benefits from extensive use of available data but lacks conclusive causal and physical explanatory skills. Hence, the causal reasons behind the relationships between surface hydrography and environmental covariates need to be interpreted with care. However, according to the model validation, the model explained well the spatiotemporal variation of surface hydrography.

AO variables and river discharge had spatially varying impacts on hydrography whereas sea ice concentration had spatially constant impact. Our results agree in general with previous studies about the spatial and temporal variation of the Kara Sea surface hydrography. The effects of AO on hydrography come through wind patterns and sea currents which control the spread of fresh water and the volume of Atlantic water entering the Kara Sea. AO index is related to climatic conditions in the Arctic and affects the sea ice and river discharge [Peterson et al., 2002; Rigor et al., 2002]. The winter mean AO affects surface hydrography through ice transport and water circulation, as suggested by the comparison of mean SST and SSS levels between negative and positive AO regimes. In this study both AO indices correlated with ice concentration and the mean winter AO correlated with the annual sum of river discharge. Despite that, we found different responses of hydrography to the covariates. Ice concentration has the least spatially varying impact on SST and SSS as monthly mean AO has a west to east varying impact and winter mean AO a south to north varying impact on SSS and SST. Discharge has the biggest effect on SSS close to the estuaries. We observed a positive trend in SST when calculating the probability for an increase in average SST from 1980-1984 to 1996-2000. Earlier studies have proved an increase of SST between years 1965 and 1995. SSS had a decreasing temporal trend that would speak for freshening of the Kara Sea. As shown here, long and short term changes of surface hydrography are shadowed by seasonality and annual fluctuations. In order to deepen our understanding of the environmental changes in the Arctic shelf areas we need to take better into account the regional and local scale patterns. The southern Kara Sea varies seasonally and is mostly affected by Atlantic currents. The northern Kara Sea is more tightly related to changes in ice formation and transport and in patterns of Arctic circulation. The continental river discharge has a local impact close to the estuaries. These regional differences affect how marine ecosystem is affected by the warming climate and by the changes in Arctic ice extent and volume.

This is the first study to present spatially and temporally detailed information about annual and seasonal variation of the hydrography in the Kara Sea and to display the spatially varying effects of environmental covariates. Our methodology is statistical and does not consider water circulation patterns as physical hydrographic models do. The benefits of the methodology are the extensive use of *in situ* measurements and the quantification of uncertainties. The study provides new, data driven, knowledge about the spatial behavior of environmental drivers of surface hydrography in an Arctic shelf sea. Furthermore, we can make spatially and temporally high resolution estimates on SST and SSS, which benefit other geophysical and ecological studies. With estimated map layers we can more accurately study the spatial dynamics of water circulation, ecosystems and species distributions.

Acknowledgments

The work was funded by the Academy of Finland (grants 292985, 266349 and 304531), the Lloyd’s Register Foundation and Research Funds of the University of Helsinki (decision No. 465/51/2014). The Lloyd's Register Foundation supports the advancement of engineering-related education, and funds research and development that enhances the safety of life at sea, on land, and in the air. We thank also the two anonymous reviewers of this manuscript who helped to significantly improve our manuscript.

The ice concentration data was generated by National Snow and Ice Data Center (NSIDC, http://nsidc.org/data/). We used the data set "Sea Ice Concentrations from Nimbus-7 SMMR and DMSP SSM/I-SSMIS Passive Microwave Data, Version 1" (Data Set ID: NSIDC-0051), which is accessible through Polaris web service (http://nsidc.org/data/polaris/). The Arctic Oscillation data was generated by NOAA Climate Prediction Center (http://www.ncdc.noaa.gov/). We utilized the data set "Monthly mean AO index since January 1950" (http://www.cpc.ncep.noaa.gov/products/precip/CWlink/daily_ao_index/ao.shtml). The bathymetry data set, International Bathymetric Chart of Arctic Ocean (IBCAO v. 3.0), is generated by several volunteer investigators. The data set is accessible through NOAA World Data Service for Geophysics (http://www.ngdc.noaa.gov/mgg/bathymetry/arctic/grids/version3_0/). The discharge data is generated by Pan-Arctic project, which goal is to generate a regional hydrometeorological data bank. We utilized the data set "Observed and naturalized discharge data for large Siberian rivers", which is accessible through R-ArcticNET v. 4.0 (http://www.r-arcticnet.sr.unh.edu/ObservedAndNaturalizedDischarge-Website/). We used the observed daily discharge values.

Supporting information holds SST and SSS map layers, which were generated with the studied methodology and with the utilized data sets.

References

Anselme, B., (1988). Monitoring of oceanic surface features in the central and south-western Kara Sea using NOAA-AVHRR imagery. In *OCEANS'98 Conference Proceedings* (Vol. 3, pp. 1657-1660). IEEE.

Boyer, T.P., et al., (2013). World Ocean Database 2013. NOAA Atlas, NESDIS 72, S. Levitus, Ed., A. Mishonov, Technical Ed.; Silver Spring, MD, 209 pp., http://doi.org/10.7289/V5NZ85MT

Cavalieri, D. J., et al., (1996), updated yearly. Sea Ice Concentrations from Nimbus-7 SMMR and DMSP SSM/I-SSMIS Passive Microwave Data, Version 1. [Sea ice concentration]. Boulder, Colorado USA. NASA National Snow and Ice Data Center Distributed Active Archive Center. doi: http://dx.doi.org/10.5067/8GQ8LZQVL0VL. [27.3.2015].

Doney, S. C., Ruckelshaus, M., Duffy, J. E., Barry, J. P., Chan, F., English, C. A., ... and Polovina, J. (2012). Climate change impacts on marine ecosystems. *Marine Science, 4*.

ESRI 2015. ArcGIS Desktop: Release 10. Redlands, CA: Environmental Systems Research Institute.

Gelfand, A. E., Kim, H. J., Sirmans, C. F., and Banerjee, S. (2003). Spatial modeling with spatially varying coefficient processes. *Journal of the American Statistical Association, 98*(462).

Gelman, A., (2006). Prior distributions for variance parameters in hierarchical models. *Bayesian analysis, 1*(3).

Gelman, A., Carlin, J. B., Stern, H. S., and Rubin, D. B. (2014). *Bayesian data analysis,* 3. edn, Chapman & Hall/CRC, Boca Raton, Florida.

Gerdes, R., (2003). Causes and development of repeated Arctic Ocean warming events. *Geophysical Research Letters, 30*(19).

Harms, I. H. and Karcher, M. J., (2005). Kara Sea freshwater dispersion and export in the late 1990s. *Journal of Geophysical Research: Oceans, 110*(C8).

Harms, I. H. and Karcher, M. J., (1999). Modeling the seasonal variability of hydrography and circulation in the Kara Sea. *Journal of Geophysical Research: Oceans, 104*(C6).

Ho, J., (2010). The implications of Arctic sea ice decline on shipping. *Marine Policy, 34*(3).

Jakobsson, M., Mayer, L., Coakley, B., Dowdeswell, J. A., Forbes, S., Fridman, B., ... and Schenke, H. W. (2012). The international bathymetric chart of the Arctic Ocean (IBCAO) version 3.0. *Geophysical Research Letters, 39*(12).

Janout, M. A., Aksenov, Y., Hölemann, J. A., Rabe, B., Schauer, U., Polyakov, I. V., ... and Kassens, H. (2015). Kara Sea freshwater transport through Vilkitsky Strait: Variability, forcing, and further pathways toward the western Arctic Ocean from a model and observations. *Journal of Geophysical Research: Oceans, 120*(7), 4925-4944.

Johnson, D. R., McClimans, T. A., King, S., and Grenness, Ø. (1997). Fresh water masses in the Kara Sea during summer. *Journal of marine systems, 12*(1), 127-145.

Lawrimore, J. H., Menne, M. J., Gleason, B. E., Williams, C. N., Wuertz, D. B., Vose, R. S., and Rennie, J. (2011). An overview of the Global Historical Climatology Network monthly mean temperature data set, version 3. *Journal of Geophysical Research: Atmospheres, 116*(D19).

Martin, S. and Cavalieri, D.J., (1989). Contributions of the Siberian Shelf Polynyas to the Arctic Ocean intermediate and deep–water. *Journal of Geophysical Research: Oceans, 94*(C89).

McClimans, T. A., Johnson, D. R., Krosshavn, M., King, S. E., Carroll, J., and Grenness, Ø. (2000). Transport processes in the Kara Sea. *Journal of Geophysical Research: Oceans, 105*(C6), 14121-14139.

McPhee, M. G., Proshutinsky, A., Morison, J. H., Steele, M., and Alkire, M. B. (2009). Rapid change in freshwater content of the Arctic Ocean. *Geophysical Research Letters, 36*(10).

Moore, S.E. and Huntington, H.P., (2008). Arctic marine mammals and climate change: impacts and resilience. *Ecological Applications*, *18*(sp2).

Morison, J. H., K. Aagaard, and M. Steele (2000). Recent environmental changes in the Arctic: A review, Arctic, 53(4), 359-371.

Morison, J. H., M. Steele, T. Kikuchi, K. Falkner, and W. Smethie (2006). Relaxation of central .Arctic Ocean hydrography to pre-1990s climatology. *Geophysical Research Letters, 33*.

Morison, J. H., R. Kwok, C. Peralta-Ferriz, M. Alkire, I. Rigor, R. Andersen, and M. Steele (2012). Changing Arctic Ocean freshwater pathways. *Nature, 481*(7379), 66-70,

Nevalainen, M., Helle, I. and Vanhatalo, J. (2016). Preparing for the unprecedented - towards quantitative oil risk assessment in the Arctic marine areas. *Marine Pollution Bulletin,* in press. doi: http://dx.doi.org/10.1016/j.marpolbul.2016.08.064

NOAA, Climate Prediction Center (30.4.2015). Daily AO index. <http://www.cpc.ncep.noaa.gov/products/precip/CWlink/daily_ao_index/ao.shtml>

NOAA, National Geophysical Data Center (30.4.2015). International Bathymetric Chart of the Arctic Ocean. < http://www.ngdc.noaa.gov/mgg/bathymetry/arctic/>

NOAA, Ocean Climate Laboratory (30.4.2015). World Ocean Data Base, <http://www.nodc.noaa.gov/OC5/WOD/pr_wod.html>

NSIDC (30.4.2015). Polaris. < http://nsidc.org/data/polaris/>

Panteleev, G., Proshutinsky, A., Kulakov, M., Nechaev, D., A. and Maslowski, W., (2007). Investigation of the summer Kara Sea circulation employing a variational data assimilation technique. *Journal of Geophysical Research: Oceans*, *112*(C4).

Pavlov, V.K. and Pfirman, S.L., (1995). Hydrographic structure and variability of the Kara Sea: Implications for pollutant distribution. *Deep-Sea Research Part II: Topical Studies in Oceanography*, *42*(6).

Peterson, B. J., Holmes, R. B., McClelland, J. W., Vörösmarty, C. J., Lammers, R. B., Shiklomanov, A. I., Shikomanov, I. A. and Rahmstorf, S., (2002). Increasing river discharge to the Arctic Ocean. *Science*, *298*(5601).

Petoukhov, V., and Semenov, V. A. (2010). A link between reduced Barents-Kara sea ice and cold winter extremes over northern continents. *Journal of Geophysical Research: Atmospheres*, *115*(D21).

Pfirman, S.L., (1995). Coastal environments of the western Kara and eastern Barents Seas. *Deep Sea Research Part II: Topical Studies in Oceanography*, *42*(6).

Polyakov, I., Timokhov, L., Dmitrenko, I., Ivanov, V., Simmons, H., Beszczynska-Möller, A., ... and Hölemann, J. (2007). Observational program tracks Arctic Ocean transition to a warmer state. *Eos, Transactions American Geophysical Union*, *88*(40), 398-399.

R-ArcticNET (30.4.2015). Observed and naturalized discharge data for large Siberian rivers. <http://www.r-arcticnet.sr.unh.edu/ObservedAndNaturalizedDischarge-Website/>

Rigor, I. G., Wallace, J. M., and Colony, R. L. (2002). Response of sea ice to the Arctic Oscillation. *Journal of Climate*, *15*(18), 2648-2663.

Rigor, I. G., and Wallace, J. M. (2004). Variations in the age of Arctic sea-ice and summer sea-ice extent. *Geophysical Research Letters*, *31*(9).

Rogers, J.C. and McHugh, M.J., (2002). On the separability of the North Atlantic oscillation and Arctic oscillation. *Climate Dynamics*, *19*(7).

Ruediger, S., (2003). *Siberian River Run-Off in the Kara Sea: Characterisation, Quantification, Variability and Environmental Significance* (Vol. 6). Elsevier.

Schauer, U., Loeng, H., Rudels, B., Ozhigin, V. K., and Dieck, W. (2002). Atlantic water flow through the Barents and Kara Seas. *Deep Sea Research Part I: Oceanographic Research Papers*, *49*(12), 2281-2298.

Shiklomanov, A.I. and Lammers, R.B., (2009). Record Russian river discharge in 2007 and the limits of analysis. *Environmental Research Letters*, *4*(4).

Simstich, J., Harms, I., Karcher, M. J., Erlenkeuser, H., Stanovoy, V., Kodina, L., Bauch, D. and Spielhagen R. F., (2005). Recent freshening in the Kara Sea (Siberia) recorded by stable isotopes in Arctic bivalve shells. *Journal of Geophysical Research: Oceans, 110*(C8).

Steele, M., & Boyd, T. (1998). Retreat of the cold halocline layer in the Arctic Ocean. *Journal of Geophysical Research: Oceans, 103*(C5), 10419-10435.

Steele, M. and Ermold, W., (2004). Salinity trends on the Siberian shelves. *Geophysical Research Letters*, *31*(24).

Steele, M., Ermold, W. and Zhang, J., (2008). Arctic Ocean surface warming trends over the past 100 years. *Geophysical Research Letters, 35*(2).

Stroeve, J., Holland, M. M., Meier, W., Scambos, T. and Serreze, M., (2007). Arctic sea ice decline: Faster than forecast. *Geophysical Research Letters*, *34*(9).

Thompson, D. W., and Wallace, J. M. (1998). The Arctic Oscillation signature in the wintertime geopotential height and temperature fields. *Geophysical research letters, 25*(9), 1297-1300.

Vanhatalo, J., Riihimäki, J., Hartikainen, J., Jylänki, P., Tolvanen, V., Vehtari, A., (2013). GPstuff: Bayesian Modeling with Gaussian Processes. *Journal of Machine Learning Research, 14*, 1175-1179.

Vehtari, A. and Ojanen J., (2012). A survey of Bayesian predictive methods for model assessment, selection and comparison. *Statistics Surveys 6*, 142-228.

Williams, C. K., and Rasmussen, C. E., (2006). Gaussian processes for machine learning. *The MIT Press*, *2*(3).

Zhang, J., Rothrock, D.A. and Steele, M., (1998). Warming of the Arctic Ocean by a strengthened Atlantic Inflow: Model results. *Geophysical Research Letters*, *25*(10).

Appendix A

Mutually independent GP priors for the spatially varying coefficients and an independent Gaussian prior for the constant coefficient (corresponding to the bathymetry) imply that the linear term of the spatially varying coefficient model (1) has a GP prior with additive covariance function

$$\boldsymbol{x}(\boldsymbol{s},t)^{\boldsymbol{T}}\boldsymbol{\beta}(\boldsymbol{s})\sim GP\left(0,k_\beta((\boldsymbol{x},\boldsymbol{s},t),(\boldsymbol{x}',\boldsymbol{s}',t'))\right), \qquad \text{(A1)}$$

where $k_\beta((\boldsymbol{x},\boldsymbol{s},t),(\boldsymbol{x}',\boldsymbol{s}',t')) = 10x_1(\boldsymbol{s},t)x_1(\boldsymbol{s}',t') + \sum_{d=2}^{4} k_d(\boldsymbol{s},\boldsymbol{s}')x_d(\boldsymbol{s},t)x_d(\boldsymbol{s}',t')$. Similarly the spatiotemporally varying intercept has a GP prior

$$\alpha(\boldsymbol{s},t)\sim GP\big(0,k_\alpha((\boldsymbol{s},t),(\boldsymbol{s}',t'))\big), \qquad \text{(A2)}$$

where $k_\alpha((\boldsymbol{s},t),(\boldsymbol{s}',t')) = 10 + k_{\text{exp}}(\boldsymbol{s},\boldsymbol{s}') + k_{\text{perST}}((\boldsymbol{s},t),(\boldsymbol{s}',t')) + k_{\text{expST}}((\boldsymbol{s},t),(\boldsymbol{s}',t')$. Hence, the spatially varying coefficient model (1) can be rewritten as a hierarchical Bayesian model

$$y(\boldsymbol{s},t)|f(\boldsymbol{s},t)\sim N(f(\boldsymbol{s},t),\sigma_\varepsilon^2) \qquad \text{(A3)}$$

$$f(\boldsymbol{s},t)|\theta\sim GP\left(0,k_\alpha((\boldsymbol{s},t),(\boldsymbol{s}',t')) + k_\beta((\boldsymbol{x},\boldsymbol{s},t),(\boldsymbol{x}',\boldsymbol{s}',t'))\right) \qquad \text{(A4)}$$

$$\theta\sim p(\theta), \qquad \text{(A5)}$$

where $f(\boldsymbol{s},t)$ denotes a latent process corresponding to the true SSS or SST at location $\boldsymbol{s}$ and time t and $p(\theta)$ denotes the prior distribution for the vector of hyper-parameters, θ, that collects all the parameters of the covariance functions $k_\alpha(\cdot,\cdot)$ and $k_\beta(\cdot,\cdot)$ (that is, all the length-scale and variance parameters) and the noise variance σ_ε^2. We gave weakly informative half Student-*t* priors [Gelman 2006] for all length-scale parameters and priors for the variance parameters of covariance functions. The observation error variance was given a log-uniform prior.

By definition, a GP prior implies that any finite number of latent variables has a multivariate Gaussian prior distribution. Hence, a vector of latent variables $\boldsymbol{f}$ corresponding to the vector of observations of SSS or SST, $\boldsymbol{y}$, has a Gaussian prior $\boldsymbol{f} \sim N(\boldsymbol{f}|0, \boldsymbol{K})$, where the entries of the covariance matrix are given by the covariance function $\boldsymbol{K}_{i,j} = k_\alpha\big((\boldsymbol{s}_i, t_i), (\boldsymbol{s}_j, t_j)\big) + k_\beta\big((\boldsymbol{x}_i, \boldsymbol{s}_i, t_i), (\boldsymbol{x}_j, \boldsymbol{s}_j, t_j)\big)$.

We optimize the hyper-parameters to their Maximum a posterior (MAP) estimate

$$\hat{\theta} = \arg\max_{\theta} p(\boldsymbol{y}|\theta)p(\theta) \qquad \text{(A6)}$$

where $p(\boldsymbol{y}|\theta) = \int N(\boldsymbol{y}|\boldsymbol{f}, \sigma_\varepsilon^2\boldsymbol{I})N(\boldsymbol{f}|0, \boldsymbol{K})d\boldsymbol{f} = N(\boldsymbol{y}|0, \boldsymbol{K} + \sigma_\varepsilon^2\boldsymbol{I})$ is the marginal likelihood of the hyperparameters. The MAP estimate was located with scaled-conjugate gradient optimization in GPstuff [Vanhatalo et al., 2012]. The MAP estimates for SST and SSS models are summarized in tables A1 and A2.

Let us denote by $\tilde{\boldsymbol{f}}$ a vector of latent variables corresponding to every grid cell and every month from 1980 to 2000. After finding the MAP estimate for the hyperparameters we calculated the (conditional) posterior predictive distribution of $\tilde{\boldsymbol{f}}$ which is again Gaussian $\tilde{\boldsymbol{f}}|\hat{\theta}, \boldsymbol{y} \sim N(\widetilde{\boldsymbol{m}}, \widetilde{\boldsymbol{K}})$. See, e.g., Rasmussen and Williams [2006] for details on how to calculate the posterior mean, $\widetilde{\boldsymbol{m}}$, and covariance, $\widetilde{\boldsymbol{K}}$. We can similarly calculate the (conditional) posterior predictive distribution for each of the components of the latent process. For example, we can calculate the posterior predictive distribution of the 2nd coefficient $\widetilde{\boldsymbol{\beta}}_{\boldsymbol{2}}|\hat{\theta}, \boldsymbol{y} \sim N(\widetilde{m}_{\boldsymbol{\beta_2}}, \widetilde{\boldsymbol{K}}_{\boldsymbol{\beta_2}})$. See Rasmussen and Williams [2006] and Gelfand et al., [2003] for details.

After solving the posterior predictive distribution for the latent variables we can calculate areal and temporal averages. For example, let $\tilde{\boldsymbol{f}}$ denote the latent variables corresponding to SST and let $\boldsymbol{w}$ be a vector of the same length as $\tilde{\boldsymbol{f}}$ so that those elements of $\boldsymbol{w}$ are $1/N$ that correspond to the N July 2000 grid cells over the Kara Sea in $\tilde{\boldsymbol{f}}$ and all other elements in $\boldsymbol{w}$ are zero. Then the July 2000 average SST over the Kara Sea has a Gaussian distribution, $\boldsymbol{w}\tilde{\boldsymbol{f}} \sim N\big(\boldsymbol{w}\widetilde{\boldsymbol{m}}, \boldsymbol{w}\widetilde{\boldsymbol{K}}\boldsymbol{w}^T\big)$. Similarly, if we want to calculate the difference between July 2000 and 1980 average SSTs we can form a vector $\boldsymbol{w_2}$ where all the elements corresponding to July 2000 have value $1/N$ and all the elements corresponding to July 1980 have a value $-1/N$; all other elements of $\boldsymbol{w_2}$ are zero. Then the difference between July average of 2000 and 1980 has a Gaussian distribution $\boldsymbol{w_2}\tilde{\boldsymbol{f}} \sim N\big(\boldsymbol{w_2}\widetilde{\boldsymbol{m}}, \boldsymbol{w_2}\widetilde{\boldsymbol{K}}\boldsymbol{w}_{\boldsymbol{2}}^T\big)$. In practice $\widetilde{\boldsymbol{K}}$ is too large (it has $(N \times 21 \times 12)^2$ elements where $N \approx 45000$) to be handled as a full matrix. Hence, we never formed full $\widetilde{\boldsymbol{K}}$ but conducted all the calculations in pieces.

Table A1. The maximum a posterior (MAP) estimate of the hyperparameters in the SST models.

Model component	hyperparameter	MAP estimate

Spatially varying coefficient of ice concentration,	Variance: σ_2^2	2.2×10^{-1}
	length-scale along s_1: $l_{2,1}$	1.0×10^3km
	length-scale along s_2: $l_{2,2}$	1.0×10^3km
Spatially varying coefficient of monthly mean AO	Variance, σ_3^2	1.7×10^{-1}
	length-scale along s_1: $l_{3,1}$	5.3×10^2km
	length-scale along s_2: $l_{3,2}$	1.0×10^3km
Spatially varying coefficient of winter mean AO	Variance, σ_4^2	1.7×10^{-1}
	length-scale along s_1: $l_{4,1}$	1.0×10^3km
	length-scale along s_2: $l_{4,2}$	1.0×10^3km
Spatially varying coefficient of log of the river Jenisei discharge	Variance, σ_5^2	2.3×10^{-1}
	length-scale along s_1: $l_{5,1}$	1.0×10^3km
	length-scale along s_2: $l_{5,2}$	1.0×10^3km
Temporally constant intercept term	Variance, σ_{exp}^2	0.1×10^{-1}
	length-scale along s_1: $l_{\text{exp},1}$	2.2×10^2km
	length-scale along s_2: $l_{\text{exp},2}$	4.8×10^2km
Unseasonal spatiotemporal term	Variance, σ_{perST}^2	0.2×10^{-1}
	length-scale along s_1: $l_{\text{perST},1}$	1.2×10^2km
	length-scale along s_2: $l_{\text{perST},2}$	1.5×10^2km
	length-scale along t: $l_{\text{perST},3}$	7.2×10^{-2}
Periodic, seasonal intercept term	Variance, σ_{expST}^2	0.2×10^{-1}
	length-scale along s_1: $l_{\text{expST},1}$	4.1×10^2km
	length-scale along s_2: $l_{\text{expST},2}$	6.9×10^2km
	length-scale along t: $l_{\text{expST},3}$	0.7×10^{-1}
Observation error (likelihood)	Noise variance, σ_ε^2	2.7×10^{-2}

Table A2. The maximum a posterior (MAP) estimate of the hyperparameters in the SSS models.

Model component	hyperparameter	MAP estimate
Spatially varying coefficient of ice concentration,	Variance: σ_2^2	9.6×10^{-2}
	length-scale along s_1: $l_{2,1}$	1.0×10^3km
	length-scale along s_2: $l_{2,2}$	1.0×10^3km
Spatially varying coefficient of monthly mean AO	Variance, σ_3^2	1.5×10^{-2}
	length-scale along s_1: $l_{3,1}$	1.0×10^3km
	length-scale along s_2: $l_{3,2}$	1.0×10^3km
Spatially varying coefficient of winter mean AO	Variance, σ_4^2	3.9×10^{-2}

	length-scale along s_1: $l_{4,1}$	1.0×10^3km
	length-scale along s_2: $l_{4,2}$	1.0×10^3km
Spatially varying coefficient of log of the river Jenisei discharge	Variance, σ_5^2	8.0×10^{-2}
	length-scale along s_1: $l_{5,1}$	1.0×10^3km
	length-scale along s_2: $l_{5,2}$	1.0×10^3km
Temporally constant intercept term	Variance, σ_{exp}^2	5.5×10^{-1}
	length-scale along s_1: $l_{\mathrm{exp},1}$	4.5×10^2km
	length-scale along s_2: $l_{\mathrm{exp},2}$	3.1×10^2km
Unseasonal spatiotemporal term	Variance, $\sigma_{\mathrm{perST}}^2$	2.0×10^{-1}
	length-scale along s_1: $l_{\mathrm{perST},1}$	1.8×10^2km
	length-scale along s_2: $l_{\mathrm{perST},2}$	1.8×10^2km
	length-scale along t: $l_{\mathrm{perST},3}$	1.0×10^{-1}
Periodic, seasonal intercept term	Variance, $\sigma_{\mathrm{expST}}^2$	9.7×10^{-3}
	length-scale along s_1: $l_{\mathrm{expST},1}$	16 km
	length-scale along s_2: $l_{\mathrm{expST},2}$	30 km
	length-scale along t: $l_{\mathrm{expST},3}$	9.4×10^{-2}
Observation error (likelihood)	Noise variance, σ_ε^2	7.7×10^{-2}

Appendix B

The purpose of the model assessment is to check the reliability of a model in order to recognize whether possible model's deficiencies have noticeable effect on the substantive inferences [Gelman et al., 2013]. Model comparison is used to assess the relative performance of alternative models and to choose the best model from them. In our application, the most important property of a model is its predictive accuracy. For this reason we use the posterior predictive checks [Gelman et al., 2013] and posterior predictive comparison [Vehtari and Ojanen, 2012] for model assessment and for choosing the best time lag for the River Yenisei discharge. Notice, here we use the term predict to refer to building probability distribution for an unseen observation, $\tilde{y}$, conditional to the training data, $\{y, x\}$, that is $p(\tilde{y}|\tilde{x}, y, x)$, whether that unseen observation was historical or in the future.

The posterior predictive check builds upon assumption that, in order for a model to work well, predictive data generated by a trained model should be similar to the measured data. We checked this first by simulating replicate measurements from the posterior predictive distribution at the same time and spatial locations as the training data and comparing the samples of $\tilde{y}$ to the measured data. We compared the replicate data with original data by sample histogram and a scatter plot between the posterior mean of replicate data and the original data. We did not find significant differences between the two.

The posterior predictive check with replicate data can be seen as a first order quality check for a model. As we are interested on models predictive performance at unseen locations and times, we conducted the model validation also using leave-one-out cross validation (LOO-CV) [Vehtari and Ojanen, 2012]. The basic idea of LOO-CV is to leave each data point at time out of the training data, train the model with the rest of the data and use the trained model to form a LOO-CV predictive distribution at the left out data point; that is $p(y_i|x_i, y_{\setminus i}, x_{\setminus i})$, where $y_{\setminus i}$ and $x_{\setminus i}$ denote all the end variables and covariates excluding the i'th data point. We compared the LOO-CV predictive mean to the left out data points with scatter plot and calculated the root mean squared error (RMSE) between the LOO-CV predictive mean and the left out data points. The RMSE of SST model was 0.2288 and that of the SSS model was 0.3314. Whereas the sample standard deviation of data y was one (since we standardized y to have standard deviation of one before modeling, see Section 3.2). Hence, the model explains 77 % of the variation in SST and 67 % in SSS. We used the LOO-CV RMSE also to choose the best time lag for the River Yenisei discharge from alternatives of 0, 1, 2 and 3 months.